ELSEVIER

Visual Observation of Two-Phase Flow Pattern of R-22, R-134a, and R-407C in a 6.5-mm Smooth Tube

Chi-Chuan Wang
Energy and Resources Laboratories, Industrial Technology Research Institute Hsinchu 310, Taiwan

Ching-Shan Chiang
Department of Mechanical Engineering, National Chiao Tung University, Hsinchu 300, Taiwan

Ding-Chong Lu
Department of Mechanical Engineering, National Chiao Tung University, Hsinchu 300, Taiwan

■ Two-phase flow pattern and friction characteristics for R-22, R-134a, and R-407C inside a 6.5 mm smooth tube are reported in this study. The range of mass flux is between 50 and 700 kg/(m^2 s). The experimental data show that the two-phase friction multipliers are strongly related to the flow pattern. For a stratified, wavy flow pattern a mass-flux dependence of the multipliers is seen. The flow pattern transition for the mixture refrigerant shows a considerable delay, compared with that of pure refrigerant. © Elsevier Science Inc., 1997

Keywords: *flow pattern, two-phase, R-22, R-134a, R-407C, pressure drops*

INTRODUCTION

A large amount of data for two-phase flow pattern has been obtained on gas–liquid two-phase flows. Most data, however, relate to air–water systems, and only limited data were available for refrigerant at higher working pressure. Hashizume [1] showed that the high-pressure two-phase flow patterns for refrigerant are quite different from those of the air–water system. In addition, the previous two-phase flow pattern studies were associated with diameters on the order of 9.5–75.0 mm, tested at mass velocities > 300 kg/(m^2 s), as illustrated by Wambsganss et al. [2]. In air-conditioning and refrigeration application, it is common to have a tube diameter less than 9.5 mm with mass velocities less than 300 kg/(m^2 s). Unfortunately, there are very few data in the open literature in this range. Furthermore, most of the available flow-pattern maps are based on the air–water system. Extension of air–water maps to the refrigerant system is doubtful. As a result, it is valuable to clarify the two-phase characteristics for refrigerants. In the present study, three refrigerants—R-22, R-134a, and R-407C—were tested. Note that R-407C is a zeotropic mixture. Its composition consists of 23 wt.% of R32, 25 wt.% of R-125, and 52 wt.% of R-134a. R-407C is a "ozone friendly" HFC refrigerant and is one of the most likely potential substitute candidates for R-22.

In the past decade, experiments on the horizontal boiling flow of refrigerant mixtures have been carried out, and heat transfer coefficients have been obtained. Reported data indicate that the heat transfer coefficients for mixture are considerably lower than those for pure refrigerant. Kedzierski et al. [3] identified several possible reasons for heat transfer degradation, including nonlinear variation of physical properties, component degradation, and circumferential and radial nonuniformity of concentration profiles. Recently, Wang et al. [4] and Kuo and Wang [5] reported a considerable decrease of heat transfer coefficients for R-407C. They suspected that the flow pattern may cause the degradation. Therefore, the key objectives of the present study are to seek an appropriate flow pattern for describing two-phase flow characteristics and to investigate their corresponding friction characteristics for R-22, R-134a, and R-407C inside a 6.5-mm tube.

EXPERIMENTAL APPARATUS

A schematic of the experimental apparatus is depicted in Fig. 1. The test apparatus is composed of three independent flow loops: namely, a refrigerant loop, a heating-water flow loop, and a glycol flow loop. The refrigerant-flow loop consists of a variable-speed gear pump that delivers subcooled refrigerant to the preheater. The refrigerant pump can provide refrigerant mass fluxes ranging from 50 to 700 kg/(m^2 s). A very accurate mass flow meter (Micromotion, model DS12S-100SU) is installed between the refrigerant pump and the preheater. The accuracy of the mass flow meter is within ±0.2% of the test span. The subcooled refrigerant liquid was heated in the preheater to obtain a prescribed inlet quality before entering the adiabatic test section. The inner diameter of the test tube is 6.5 mm, and the length of the smooth tube is 1200 mm.

Address correspondence to *Chi-chuan Wang*, D200 ERL/ITRI, Bldg. 64, 195–6 Section 4, Chung Hsing Rd., Chutung, 310, Hsinchu, Taiwan.

Experimental Thermal and Fluid Science 1997; 15:395–405

655 Avenue of the Americas, New York, NY 10010

0894-1777/97/$17.00
PII S0894-1777(97)00007-1

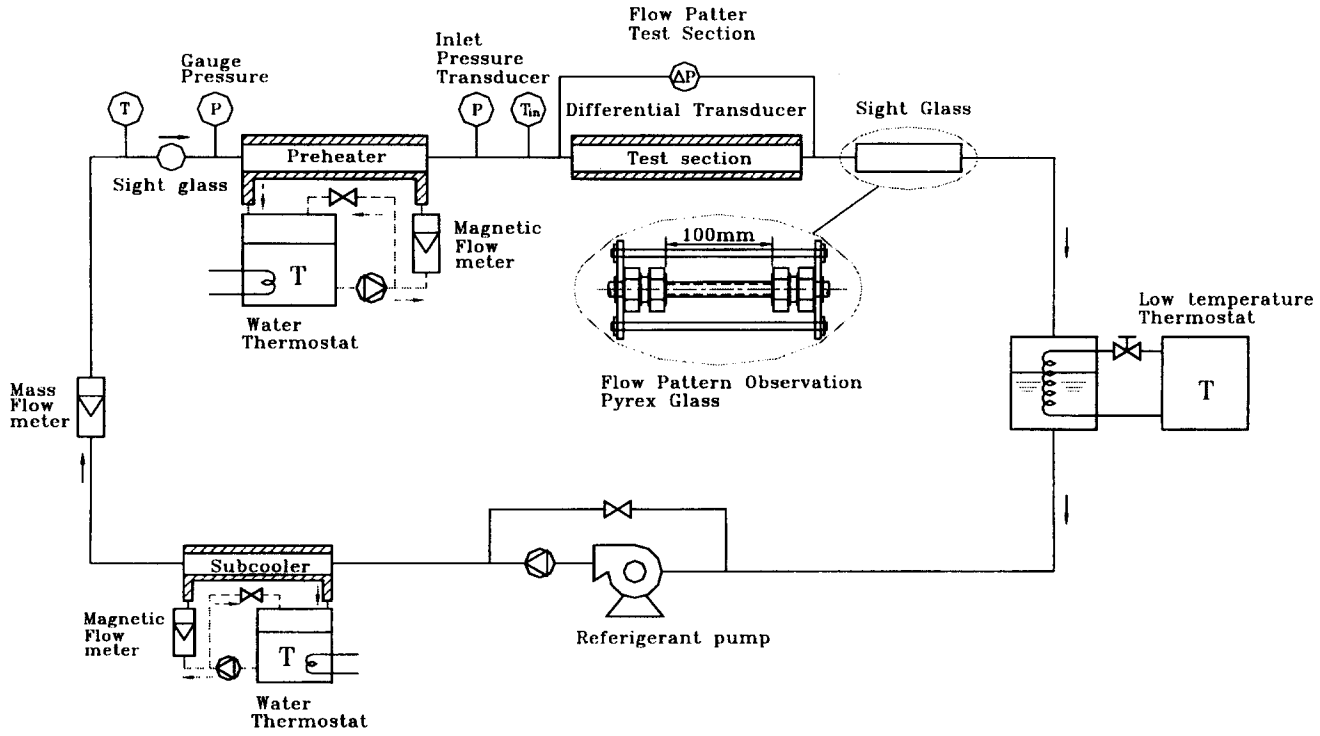

Figure 1. Schematic representation of test apparatus.

The test tube is well insulated by 50-mm-thick rubber having a thermal conductivity of 0.032 W/(m K). During the experiments, the saturation temperatures were fixed at 2, 6 and 20°C, respectively. The pressure drops of the refrigerant were measured at a YOKOGOWA EJ110 having an adjustable span from 1300 to 13,000 Pa. Resolution of this pressure differential pressure transducer is 0.3%. The refrigerant leaving the test section was connected to a Pyrex sight glass having an inside diameter identical with that of the test section. The sight glass has a length of 100 mm and an internal diameter of 6.5 mm. Flow patterns are obtained from direct visual observations made with microcamera (Nikon FM2) having extension tubes of 13 mm + 21 mm + 31 mm. The exposure time of the microcamera during the tests ranges from 1/2000 to 1/4000 s, and the corresponding aperture is 4. A Brom cine light (500 W) was used in taking photographs. On leaving the test section, the refrigerant was condensed and subcooled by glycol circuit. The refrigerant temperatures were measured by a resistance temperature device (Pt 100 Ω) having a calibrated accuracy of 0.05C° (calibrated by an HP quartz thermometer probe with a quartz thermometer, models 18111A and 2804A). The inlet temperature of the glycol is controlled by a thermostat. Both the thermodynamic and the transport properties of R-22, R-134a, and R-407C are evaluated by using a computer program (REFPROP 1996) [6]. The uncertainties reported in this study, in accord with the single-sample analysis proposed by Moffat [7], are tabulated in Table 1.

FLOW VISUALIZATION

Considerable differences exist in the definitions of two-phase flow patterns. Because flow pattern identification by visual observation is subjective, it is essential that the flow patterns be defined in detail. In accord with the classification by Taitel [8], the basic flow patterns inside a horizontal tube are divided into four main classes:

1. Stratified flow: the liquid flows at the bottom of the pipe with gas at the top. This flow pattern can be

Table 1. Summary of Estimated Uncertainties

Primary Measurements		*Derived Quantities*		
Parameter	*Uncertainty*	*Parameter*	*Uncertainty* (G = 50 kg / m^2 s)	*Uncertainty* (G = 700 kg / m^2 s)
$\dot{m}_r$	0.3–1%	G	1.1%	0.5%
ΔP	2.7%	ϕ_v^2	±16.1%	±5.6%
T	0.05C°	x	±3.1%	±1.1%
		X	±6.4%	±2.8%

subdivided into stratified smooth (statified) and stratified wavy (wavy) flow pattern.
2. Intermittent flow: the flow is in the form of liquid slugs that fill the pipe and are separated by gas zones in the form of elongated bubbles; a stratified liquid layer flows along the bottom of the pipe. This flow pattern can be subdivided into plug and slug flow.
3. Annular flow: a liquid film flows adjacent to the pipe wall, and gas flows in the center core.
4. Bubble flow: small discrete bubbles are distributed in a continuous liquid phase.

PRESSURE DROP DATA REDUCTION

The pressure drop data were analyzed by using the concept of the two-phase multiplier. Tests were conducted adiabatically in the flow pattern observation test section. Because the acceleration pressure gradient, ΔP_a, can be neglected in the adiabatic experiments, a more accurate calculation of the frictional multiplier can be obtained. The multiplier is defined by

$$\phi_v^2 = \frac{dP_f/dz}{dP_{f,G}/dz}, \quad (1)$$

where dP_f/dz is the measured two-phase frictional pressure gradient and $dP_{f,G}/dz$ is the frictional pressure gradient corresponding to vapor flowing alone in the channel. The multiplier is typically plotted versus quality x or the Martinelli parameter X, where

$$X = \sqrt{\frac{(dP_{f,L}/dz)}{(dP_{f,G}/dz)}}. \quad (2)$$

To verify the instrumentation and the measurement results, single-phase pressure drops for R-22, R-134a, and R-407C were measured, and a plot of the friction factor versus the Reynolds number is shown in Fig. 2. The baseline is the Blasius friction factor equation ($0.079Re_{Di}^{-0.25}$). For $Re_{Di} > 10{,}000$, the deviations between the present experimental data and the Blasius correlation are within 6%. The good agreement shown in Fig. 2 substantiate the validity of the instrumentation and the experimental apparatus.

RESULTS AND DISCUSSION

Photographs representative of the observed flow patterns for R-22 and R-407C and corresponding to mass-flow velocities of 100, 200, 400, and 700 kg/(m^2 s) are presented in Fig. 3, to show the progression from one flow pattern to the next. The corresponding saturation temperature is 20°C. Note that the flow patterns for R-134a are not shown, because its flow pattern is very similar to that of R-22. The main liquid–vapor interface is the white line. The flow patterns for G = 100 kg/(m^2 s) include the plug, slug, and stratified flow pattern (stratified smooth and stratified wavy). Note that the annular flow pattern is not seen for a mass velocity of 100 kg/(m^2 s). A further increase in mass velocities to G = 200 and 400 kg/(m^2 s) results in plug/slug, stratified, wavy, and annular patterns. For a fixed mass flux, the flow-pattern progression vs quality for R-22 and R-407C is considerably different. Interestingly the flow pattern progression for R-407C falls behind that of R-22. For instance, for G = 200 kg/(m^2 s) and x = 0.703, the flow pattern for R-22 is annular, whereas the flow pattern for R-407C is wavy. For G = 400 kg/(m^2 s) and x = 0.1, the flow pattern for R-22 is wavy, whereas that for R-407C is slug.

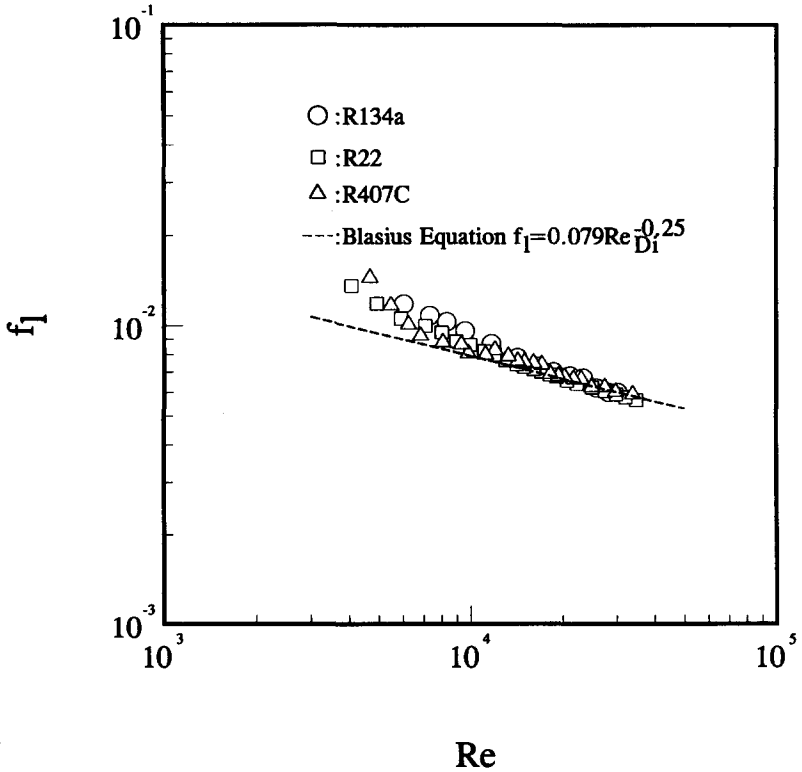

Figure 2. Subcooled liquid friction factors compared with Blasius equation.

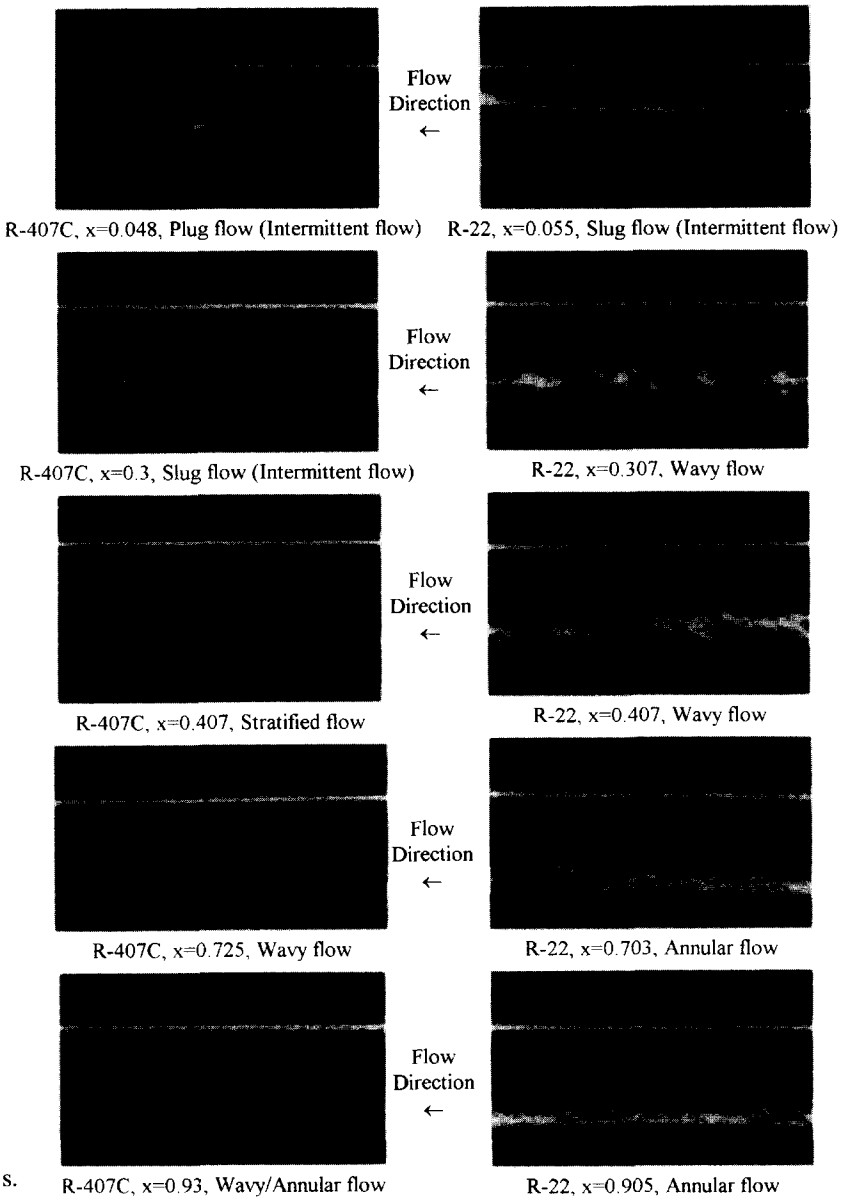

Figure 3(*a*). Flow pattern for $G = 100$ kg/m^2 s.

An explanation for this phenomenon can be described as follows. At the initial stage of evaporation (low-quality region), the more-volatile components R-32 and R-125, evaporated faster than that of the least-volatile component, R-134a. As a results, the vapor phase may contain more R-32 and R-125 compared with the initial concentration. Refer to the physical properties for R-32, R-125, and R-134a in Table 2. Notice that the properties are obtained from the REFPROP program [6]. One can easily find that ρ_G for R-32 is 40.7 kg/m^3, which is 46.7% higher than that for R-134a, and ρ_G for R-125 is 77.83 kg/m^3, 280% higher than that for R-134a; ρ_L for R-32 is 981.7 kg/m^3, which is 20% lower than that for R-134a, and ρ_L for R-125 is about the same as that for R-134a. Considering a fixed mass flux ($G = \rho u$), the higher mean density of vapor phase due to the contribution of R-32 and R-125 results in a lower mean vapor-phase velocity. The least-volatile component, R-134a, increased the concentration of the liquid phase throughout the evaporation process (in both low- and high-quality regions). Consequently, the higher mean density of the liquid phase due to R-134a again suggests a lower mean liquid velocity. Therefore, compared with R-22, lower mean gas- and liquid-phase velocities are likely for the mixture R-407C. Furthermore, the liquid viscosity for R-134a is approximately 80% higher than that of the most-volatile component, R-32. As R134a increases concentration of the liquid phase, it also contributes to decreasing the liquid-phase mean velocity. As a result, the variation in density and viscosity may delay the flow-pattern transition for R-407C compared with pure refrigerant R-22.

The liquid entrainment is clearly seen for the wavy and annular flow patterns for R-22 and $G = 200$ kg/(m^2 s). However, for the same mass flux for R-407C, the quantity of liquid entrainment is considerably less than that of R-22. Entrainment is associated with the disturbance between the vapor and the liquid interface. The entrainment rate heavily depends on both gas- and liquid-phase veloci-

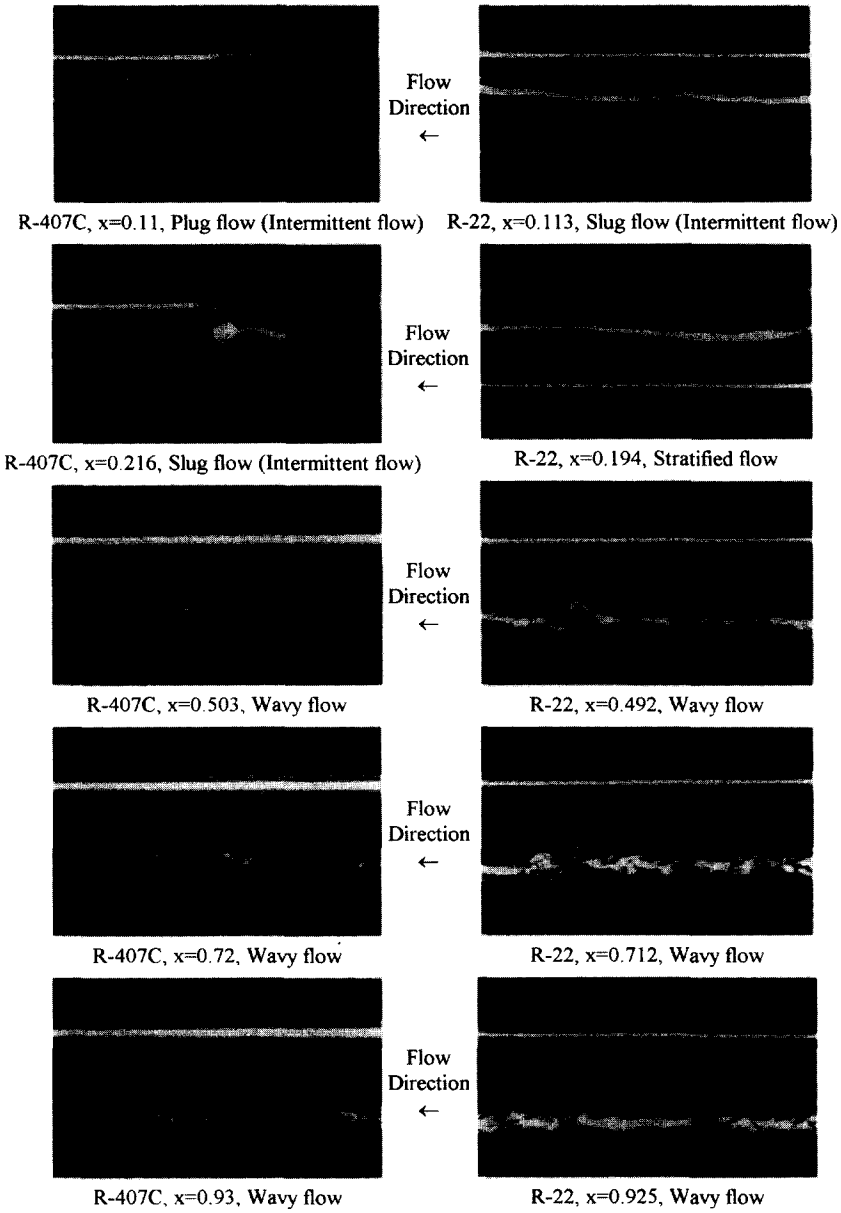

Figure 3(*b*). Flow pattern for $G = 200$ kg/m^2 s.

ties. As mentioned earlier, the gas- and liquid-phase velocities for R-407C may be much lower than those of R-22. Eventually, the liquid entrainment for R-407C is expected to be lower than that for R-22. In addition, the variation in the local properties of R-407C may contribute to this phenomenon. As suggested by Govan et al. [9], the onset of entrainment is related to the property index $(\mu_G/\mu_L)(\rho_L/\rho_G)^{1/2}$, exponentially. Initially, this value is 0.395 for R-22 and 0.4065 for R-407C. As evaporation proceeds, the liquid phase for R-407C becomes richer in the less-volatile component R-134a. A detailed estimation of this value may decrease to 0.307 in the worst condition. Thus the liquid entrainment for R-407C is considerably less than for R-22.

The flow patterns for $G = 400$ and 700 kg/(m^2 s) include the slug, wavy-annular, and annular flow patterns. As seen, the annular flow pattern becomes the dominate flow pattern as mass flux increase. The development of the flow pattern for R-407C, again, falls behind that for R-22.

The present flow-pattern data were compared with several flow-patter maps, including those of Baker [10], Mandhane et al. [11], VDI [12], and Weisman et al. [13]. The VDI flow-patter map is a modified flow-pattern map of the well-known semiempirical flow pattern map proposed by Taitel and Dukler [14]. In summary, the flow-pattern map proposed by Weisman shows the highest predictability (85%), the Baker map shows 59%, the VDI map shows only 38%, and the Mandhane map shows the poorest prediction (12%). The Weisman flow-pattern map [13] includes extensive new data on the transitions between two-phase flow patterns during concurrent gas-liquid flow in horizontal lines. Systematic studies on the effects of liquid viscosity, liquid density, surface tension, gas density, and tube diameter were reported in this study. Weisman et al. [13] proposed revised dimensionless corre-

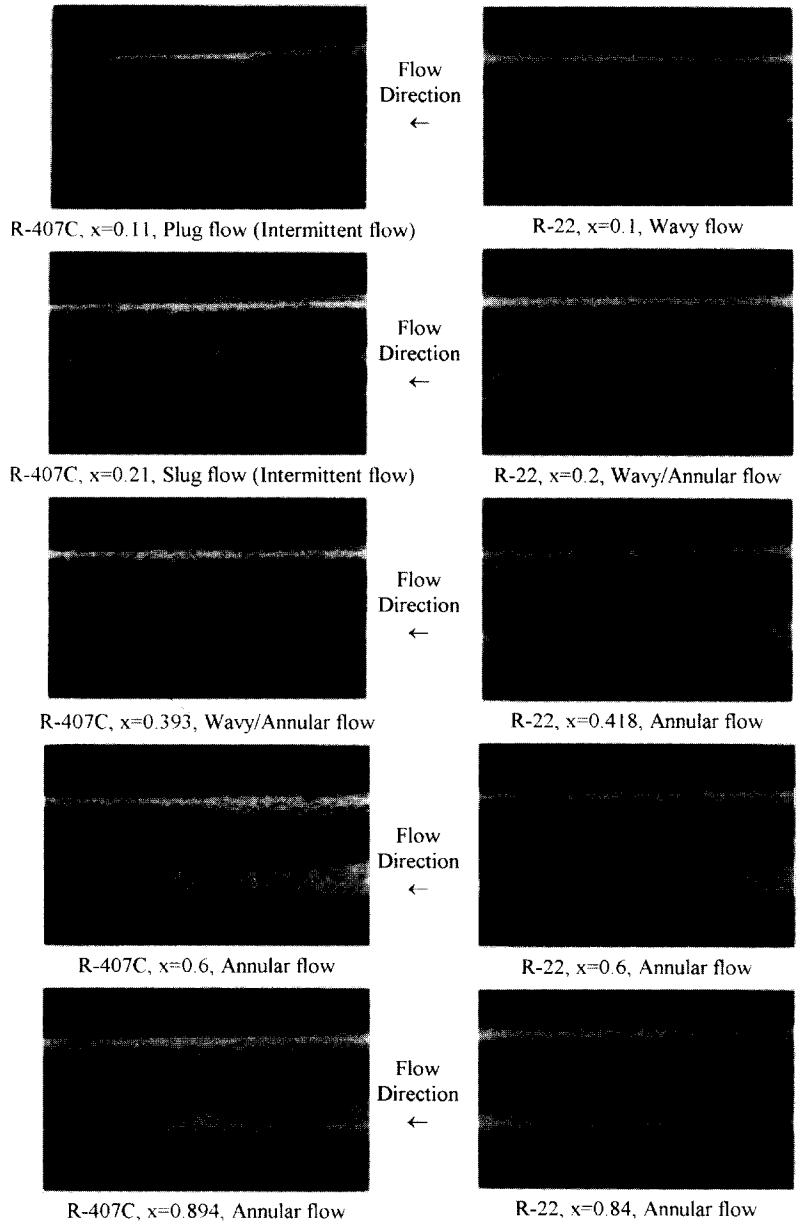

Figure 3(*c*). Flow pattern for $G = 400$ kg/m^2 s.

lations that successfully fit their own data and previously available data. The present experimental data can be described by the flow-pattern map very well. It seems, however, that the flow-pattern map of Weisman et al. [13] may not be straightforward form an engineering point of view because it requires complex transition equations. The Baker flow-pattern map is one of the most widely used because it is easy to use. The Baker flow-map proposes two property correction factors:

$$\lambda = \left(\frac{\rho_G}{\rho_A}\frac{\rho_L}{\rho_W}\right)^{1/2}, \tag{3}$$

$$\psi = \left(\frac{\sigma_W}{\sigma}\right)\left[\left(\frac{\mu_L}{\mu_W}\right)\left(\frac{\rho_W}{\rho_L}\right)^2\right]^{1/3}. \tag{4}$$

Hashizume [1] noted that the surface tension correction in Eq. (4) may be overemphasized for refrigerants R-22 and R-12. He suggested a modification of ψ—namely,

$$\psi' = \left(\frac{\sigma_W}{\sigma}\right)^{1/4}\left[\left(\frac{\mu_L}{\mu_W}\right)\left(\frac{\rho_W}{\rho_L}\right)^2\right]^{1/3}. \tag{5}$$

Hashizume [1] successfully classified his experimental data for R-12 and R-22 in a 10-mm smooth tube by using the modified Baker flow-pattern map. A detailed examination of the present refrigerant data supports the findings of Hashizume [1]. Figure 4 shows the present experimental data for R-22, and R-134a plotted against $((1 - x)/x)\lambda\psi'$. The original transition lines proposed by Hashizume [1] also are shown in Fig. 4. As can be seen, both the wavy-to-annular transition line and the stratified-to-wavy flow pattern are slightly lower than those of Hashizume [1]. This may be due to the larger tube diameter (10 mm) used by Hashizume [1] compared with

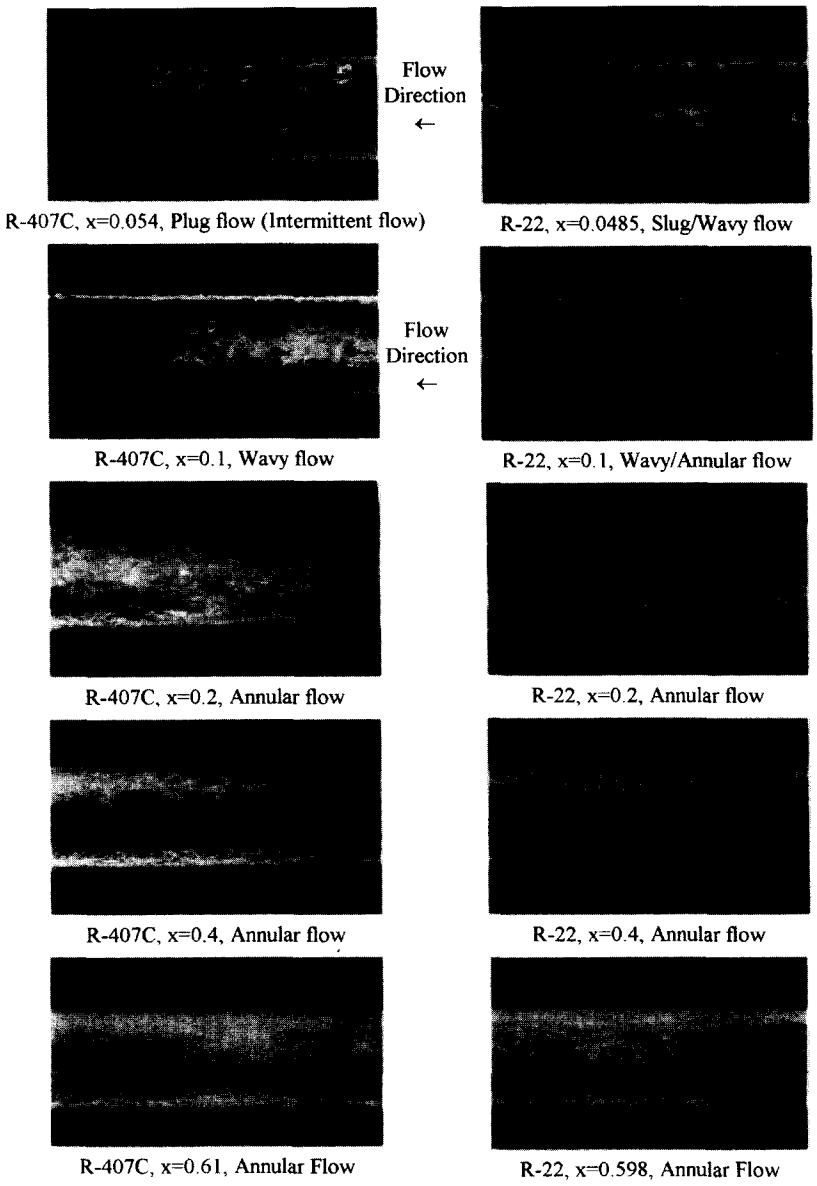

Figure 3(*d*). Flow pattern for $G = 700\ \text{kg/m}^2\ \text{s}$.

the present data. The flow pattern for R-407C is shown in Fig. 5. As can be seen, the transition from the intermittent to the annular flow pattern is shifted. As explained earlier, local variation in properties change the flow pattern. Note that the surface-tension data for R-407C are not available in the literature. A simple linear mole fraction weighting method is used; that is,

$$\sigma_{\text{R407C}} = 0.25\sigma_{\text{R125}} + 0.23\sigma_{\text{R32}} + 0.52\sigma_{\text{R123a}}. \quad (6)$$

Although there are other more complicated methods for calculating the mole fraction weight, Jung [15] argued that the simple method has proved to be as good as the others.

Lockhart and Martinelli [16] correlated the two-phase multipliers, ϕ_v^2, in terms of a parameter, now called the Lockhart-Martinelli parameter defined in Eq. (2). Chisholm [17] proposed the following relation for a round, smooth tube:

$$\phi_v^2 = 1 + CX + X^2. \quad (7)$$

For smooth tubes, the constant C ranges from 5 to 20, depending on whether the liquid and vapor phases are laminar or turbulent. In particular, the C factor can be

Table 2. Physical Properties for R-32, R-125, R-134a, R-22, and R-407C Evaluated at 20°C

Property	*R-32*	*R-125*	*R-22*	*R-134A*	*R-407C*
ρ_L, kg/m^3	981.7	1219	1210	1225	1162
ρ_G, kg/m^3	40.70	77.83	38.91	27.76	37.15
ρ_L/ρ_G	24.1	15.66	31.1	44.13	31.28
μ_L, 10^{-6}Pa-s	125	154.4	180.8	224.7	172.1
μ_G, 10^{-6}Pa-s	12.57	13.97	12.81	11.92	12.51
μ_L/μ_G	9.94	11.1	14.11	18.85	13.76
i_{fg}, kJ/kg	282.5	115.5	185.2	182.5	191.4

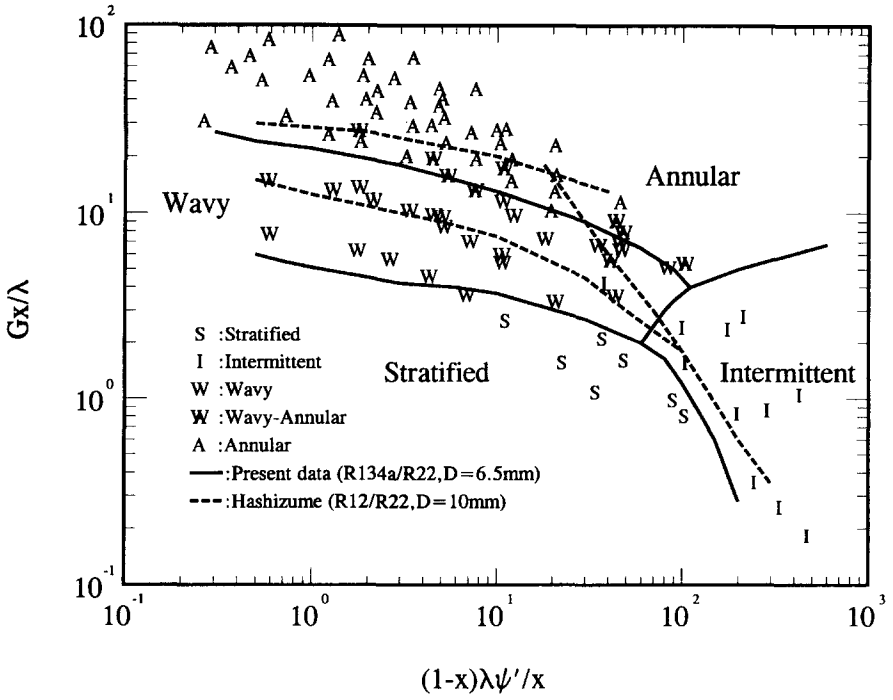

Figure 4. Comparison of the present flow pattern data, using modified Baker map (R-22 & R-134a).

adjusted to give a best fit to a given set of data. Figure 6 shows the measured data for pure refrigerants (R-22 and R-134a) plotted in the form ϕ_v^2 vs X and those predicted by Eq. (7) for $C = 5$ and 20. Actually, C is strongly related to the observed flow pattern. For pure refrigerant R-22 and R-134a, as seen in Fig. 6, the present experimental data show that a constant of $C = 5$ may be more appropriate for the intermittent flow pattern, and this it true even if the Reynolds numbers of both vapor and liquid phases are turbulent. For a mass velocity greater than 200 kg/(m^2 s), the two-phases are turbulent, and the two-phase multipliers were insensitive to the change in mass velocity. This corresponds to the wavy-annular flow pattern. However, for a mass velocity of 50 and 100 kg/(m^2 s), the experimental data show a pronounced effect of mass velocity. This may be explained by the wavy flow pattern in Fig. 3*a*. For $G = 100$ kg/(m^2 s), the shear force at the vapor–liquid interface is not large enough; therefore the amplitudes of the wave cannot reach the top of the tube. This implies a partially wet phenomenon. Therefore, the

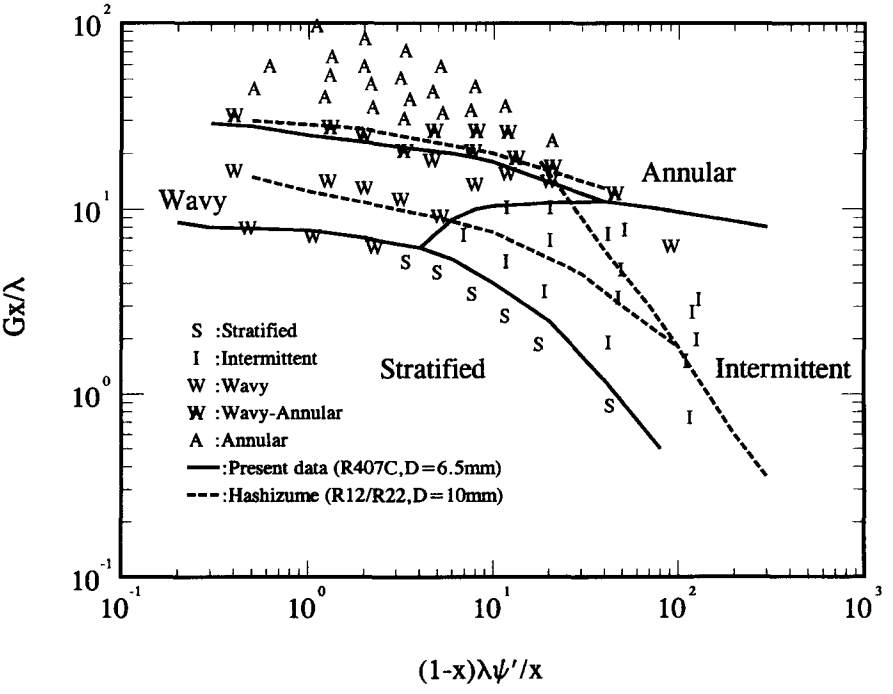

Figure 5. Comparison of the present flow pattern data, using modified Baker map (R-407C).

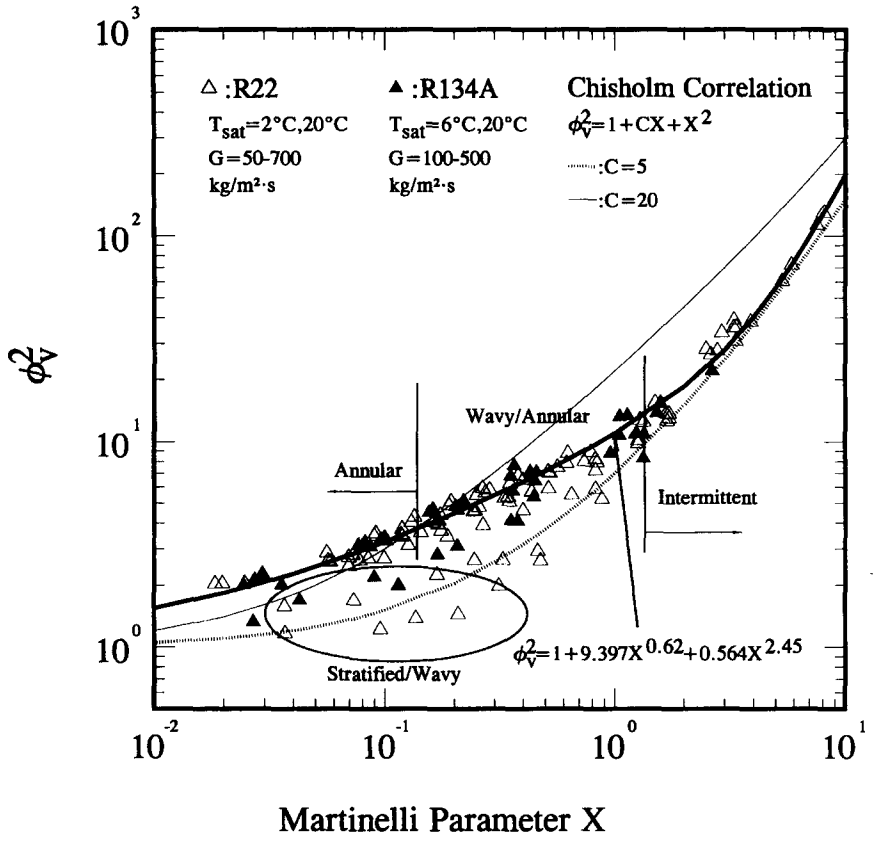

Figure 6. Frictional multiplier vs Martinelli parameter for the experimental data (R-22 and R-134a).

friction characteristics may depend on the wetted perimeter, which is affected by the mass velocity. For $G > 200$ kg/(m^2 s), the amplitude of the observed wavy flow pattern becomes high enough to reach the top. Although the main flow pattern is wavy, the two-phase flow characteristics can be regarded as completely wet. Therefore, the effect of mass flux on two-phase multipliers decreased.

With the use of multiregression process, the multiplier for $G \geq 200$ kg/(m^2 s) can be correlated as

$$\phi_v^2 = 1 + 9.4X^{0.62} + 0.564X^{2.45}. \quad (8)$$

Note that Eq. (8) can correlate 91% of the data having mass velocities higher than 200 kg/(m^2 s) within $\pm 20\%$. Also shown in the Fig. 6 is that, at mass velocities of 50 and 100 kg/(m^2 s), the two-phase multipliers are quite different from the prediction by Eq. (8). The mass flux shows a considerable effect on the two-phase multiplier. Consequently, the C factor is not a constant by a function of the Martinelli parameter, mass flux, and other physical properties. The experimental data of Wambsganss et al. [18] and Kuo and Wang [19] also indicate this phenomenon. They proposed a modification on the C factor by using the Chisholm correlation [17], and the modified expression of C is given by

$$C = C(X, Re_{LO}) = aX^b. \quad (9)$$

Therefore, with the use of a multiregression process, the C value for the present experimental data for R-22 and R-134a for T_{sat} = 20, 6, and 2°C can be correlated as

$$C = 0.000004566X^{0.128}\mathrm{Re}_{LO}^{0.938}\left(\frac{\rho_L}{\rho_G}\right)^{-2.15}\left(\frac{\mu_L}{\mu_G}\right)^{5.1}. \quad (10)$$

Equation (10) can describe 85% of the data within $\pm 20\%$.

The two-phase multipliers for mixture refrigerant R-407C are presented in Fig. 7. As is seen, the multipliers for R-407C are notably lower than those for pure refrigerants. In addition, the multipliers for R-407C are quite scattered. This phenomenon may be attributed to the local variation in physical properties and to the delay in the transition form one flow pattern to another. Furthermore, the physical properties of R-407C are evaluated at the initial concentration. In the actual evaporation process, the physical properties change with the vapor quality. However, correctly keeping track of the physical properties for different vapor qualities may not be possible.

PRACTICAL SIGNIFICANCE

R-22 and R-134a refrigerants are widely used in heating, ventilating, and air-conditioning systems, as well as in refrigerators, and R-407C is a potential substitute for R-22. The modified flow-pattern maps for pure refrigerants and mixtures herein presented herein may be used by designers. The mixture refrigerant R-407C revealed very interesting characteristics for the delay of transition to another flow pattern, which may explain the degradation of heat transfer. Thus, the present study enhances understanding of the two-phase flow in small pipes, which

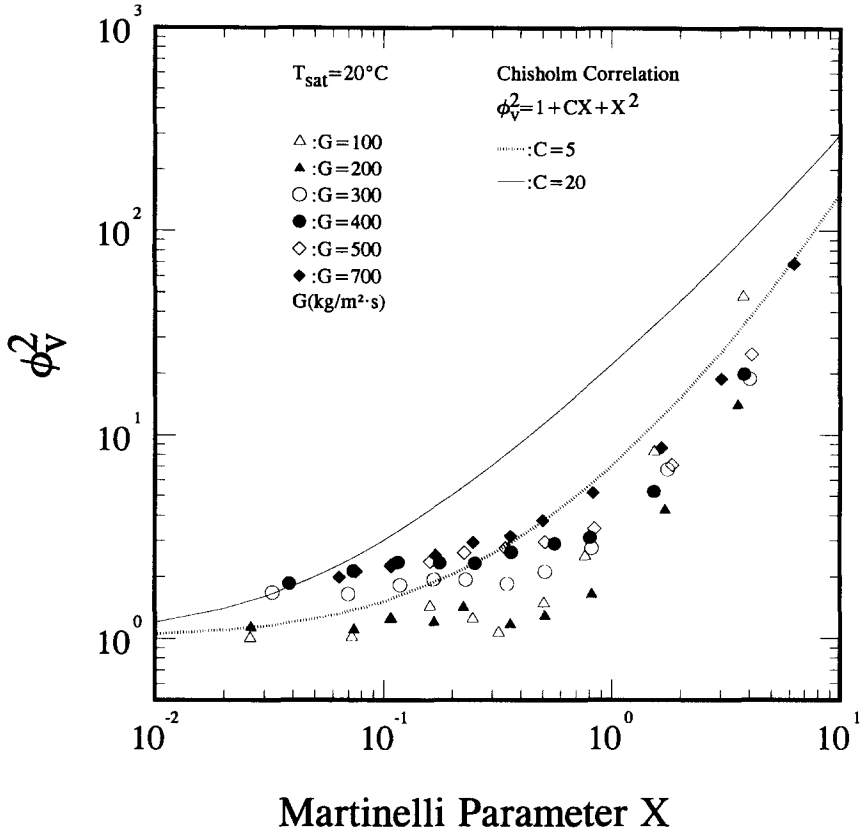

Figure 7. Frictional multiplier vs Martinelli parameter for experimental data (R-407C).

may be incorporated into better design and more reliable products.

CONCLUDING REMARKS

Two-phase flow patterns and friction characteristic of R-22, R-134a, and R-407C inside a 6.5-mm smooth tube are reported in this study. The range of mass flux is between 50 and 700 kg/(m^2 s). Conclusions of the present study are as follows:

1. The two-phase multipliers are strongly related to the flow pattern, and the two-phase multiplier depends on mass velocities for the partially wet stratified-wavy flow pattern. For intermittent, annular-wavy, and annular flow patterns, the two-phase multipliers are insensitive to changes in mass flux.
2. The mixture refrigerant, R-407C, reveals a delay of flow-pattern transition due to local variation in the physical properties of density and viscosity. Consequently, the two-phase multipliers for the mixture refrigerant are considerably lower than those for pure refrigerant.
3. The onset of liquid entrainment of R-407C is much slower than that of pure refrigerant, and the quantity of the entrainment is much less than that of pure refrigerant.

The authors would like to express gratitude for the Energy R & D foundation funding from the Energy Commission of the Ministry of Economic Affairs in support of this research.

NOMENCLATURE

C	constant in Chisholm correlation
dP_f/dZ	measured two-phase frictional pressure gradient, N/m^2
$dP_{f,l}/dZ$	frictional pressure gradient for liquid flowing alone, N/m^2
$dP_{f,v}/dZ$	frictional pressure gradient for gas flowing alone, N/m^2
ΔP_a	pressure drop due to acceleration, N/m^2
ΔP_f	frictional pressure drop, N/m^2
D_i	inside diameter of the tube, m
f_l	friction factor for subcooled liquid, dimensionless
G	mass flux, kg/(m^2 s)
i_{fg}	latent heat, kJ/kg
L	effective heating length, m
$\dot{m}_r$	average mass flow rate of refrigerant, kg/s
Re_{LO}	Reynolds number for liquid flow only, dimensionless
T_{sat}	saturation temperature of the refrigerant, °C
v	average specific volume, m^3/kg
x	vapor quality
X	Martinelli parameter

Greek Symbols

ρ	density of refrigerant, kg/m^3
ϕ_v^2	two-phase friction multiplier for vapor flowing alone
μ	dynamic viscosity of refrigerant, N s/m^2

ν kinematic viscosity of refrigerant, T/s
σ surface tension of refrigerant, N/m

Subscript

A air properties evaluted at 1 atm, 20°C
L liquid phase for refrigerant
G gas phase for refrigerant
R134a R-134a
R22 R-22
R407C R407C
W water properties evaluated at 1 atm, 20°C

REFERENCES

1. Hashizume, K., Flow Pattern and Void Fraction of Refrigerant Two-Phase Flow in a Horizontal Pipe. *Bull. JSME* **26**, 1597–1602, 1983.
2. Wambsganss, M. W., Jendrzejczyk, J. A., and France, D. M., Two-phase Flow Pattern and Transition in a Small, Horizontal Rectangular Channel, *Int. J. Multiphase Flow* **17**(3), 327–342, 1991.
3. Kedzierski, A., Kim, J. H., and Didion, D. A., Cause of Apparent Heat Transfer Degradation for Refrigerant Mixtures. Two-Phase Flow and Heat Transfer ASME HTD-197, pp. 149–158, 1992.
4. Wang, C. C., Kuo, C. S., Chang, Y. J., and Lu, D. C., Two-Phase Heat Transfer and Friction Characteristics of R-22 and R-407C. *ASHRAE Trans.* **102**(1), 830–838, 1996.
5. Kuo, C. S., and Wang, C. C., Horizontal Flow Boiling of R22 and R407C in a 9.52 mm Micro-Fin Tube. *Appl. Thermal Eng.* **16**(8/9), 719–731, 1996.
6. *REFPROP: Thermodynamic Properties of Refrigerants and Refrigerant Mixtures*. Version 5.0, National Institute of Standards and Technology, Gaithersburg, MD, 1996.
7. Moffat, R. J., Describing the Uncertainties in Experimental Results. *Exp. Thermal Fluid Sci.* **1**, 3–17, 1988.
8. Taitel, Y., Flow Pattern Transition in Two-Phase Flow. Presented at *Ninth Int. Heat Transfer Conference*, Jerusalem, pp. 237–254, 1990.
9. Govan, A. H., Hewitt, G. F., Owen, D. G., and Bott, T. R., An Improved CHF Modelling Code. *Second UK Nat. Conf. Heat Transfer* **1**, 33–48, 1988.
10. Baker, O., Design of Pipe Lines for Simultaneous Flow of Oil and Gas. *Oil Gas J.* **53**, 185–195, (1954).
11. Mandhane, J. M., Gregory, G. A., and Aziz, K. A., A Flow Pattern Map for Gas-Liquid Flow in Horizontal Pipeline. *Int. J. Multiphase Flow* **1**, 537–553, 1974.
12. VDI-Warmeatlas Heat Transfer to Boiling Saturated Liquids. In *VDI Heat Atlas*, Chap. Hbb1, VDI-Verlag GmbH, Germany, 1993, (in English).
13. Weisman, J., Duncan, D., Gibson, J., and Crawford, T., Effect of Fluid Properties and Pipe Diameter on Two-Phase Flow Pattern in Horizontal Lines. *Int. J. Multiphase Flow* **5**, 437–462, 1979.
14. Taitel, Y., and Dukler, A. E., A Model for Prediction of Flow Regime Transitions in Horizontal and Near Horizontal Gas-Liquid Flow. *AIChE J.* **22**, 47–55, 1976.
15. Jung, D. G., Mixtures Effects on Horizontal Convective Boiling Heat Transfer. Ph.D. Thesis, Univ. Maryland, College Park, MD, 1988.
16. Lockhard, R. W., and Martinelli, R. C., Proposed Correlation of Data for Isothermal Two-Phase Two-Component Flow in Pipes. *Chem. Eng. Prog.* **45**, 39–49, 1949.
17. Chisholm, D., Pressure Gradient Due to Friction During the Flow of Evaporating Two-Phase Mixtures in Smooth Tube and Channels. *Int. J. Heat Mass Transfer* **16**, 347–348, 1973.
18. Wambsganss, M. W., Jendrzejcyk, J. A., France, D. M., and Obot, N. T., Friction Pressure Gradients in Two-Phase Flow in a Small Horizontal Rectangular Channel. *Exp. Thermal Fluid Sci.* **5**, 40–56, 1992.
19. Kuo, C. S., and Wang, C. C. In-Tube Evaporation of HCFC-22 in a 9.52mm Micro-Fin/Smooth Tube. *Int. J. Heat Mass Transfer* **39**(12), 2559–2569, 1996.

Received July 12, 1996; revised December 7, 1996